

## Article

# Design and Operation Parameters of Vibrating Harvester for *Coffea arabica* L.

Yingjie Yu, Ying Cao, Qinghui Lai \*, Qinghui Zhao, Zhexing Sun , Shengwu Zhou and Dake Song

Faculty of Modern Agricultural Engineering, Kunming University of Science and Technology, Kunming 650500, China

\* Correspondence: laiqinghui@kust.edu.cn

**Abstract:** This study designed a handheld vibrating coffee harvester to improve the mechanized harvesting of *Coffea arabica* L. The proposed device was used to vibrate branches of *Coffea arabica* L. trees, and the shedding of coffee fruit and the operation parameters of vibrational harvesting were analyzed. Images captured using high-speed photography were used to derive a force equation that represents the forced vibration of the coffee fruit-stalk joint. In addition, the vibrations of coffee berries and branches were theoretically analyzed, and the results were used to establish a dynamic vibration model of coffee trees. The shedding of coffee berries was primarily affected by the vibration frequency, vibration amplitude, and excitation position, which were simulated using a rigid–flexible branch-machine coupling model on RecurDyn software. Furthermore, field experiments were conducted to determine the optimal working parameters for coffee harvesting using vibrations. The results indicated optimal picking performance when the vibration frequency, vibration amplitude, and excitation position were 62 Hz, 9 mm, and 0.4 L, respectively. The harvesting rates of ripe and unripe coffee were 92.22% and 8.33%, respectively, and the damage rate was 5.23%. Thus, the proposed harvester can satisfactorily achieve the optimal harvesting of *Coffea arabica* L.

**Keywords:** *Coffea arabica* L.; picking device; vibrating; fruit-stalk-branch model; RecurDyn



**Citation:** Yu, Y.; Cao, Y.; Lai, Q.; Zhao, Q.; Sun, Z.; Zhou, S.; Song, D. Design and Operation Parameters of Vibrating Harvester for *Coffea arabica* L.. *Agriculture* **2023**, *13*, 700. <https://doi.org/10.3390/agriculture13030700>

Academic Editor: Galibjon M. Sharipov

Received: 22 February 2023

Revised: 15 March 2023

Accepted: 16 March 2023

Published: 17 March 2023



**Copyright:** © 2023 by the authors. Licensee MDPI, Basel, Switzerland. This article is an open access article distributed under the terms and conditions of the Creative Commons Attribution (CC BY) license (<https://creativecommons.org/licenses/by/4.0/>).

## 1. Introduction

*Coffea arabica* L. is a small-grain coffee species of the Rubiaceae family with a tropical evergreen tree. The unique climatic and natural conditions of Yunnan Province, China, are suitable for coffee cultivation, and the coffee grown in that region is popular in the international market. In 2020, the coffee plantation area in Yunnan was 135,000 hm<sup>2</sup> [1,2] and accounted for approximately 98% of the country's total production. The existing methods for harvesting small-grain coffee in China are entirely manual and are thus expensive and inefficient, impeding the sustainable development of the coffee industry [3]. Therefore, research efforts should be dedicated to developing efficient coffee harvesting methods and machinery that apply to hilly mountainous areas.

Studies focused on mechanized coffee harvesting have revealed that self-propelled coffee harvesting machines manufactured by Oxbo, Brastoft, and Case have high harvesting efficiency; however, a large proportion of the harvested fruit is green, and the machines are massive and thus are unsuitable for hilly and mountainous operating conditions [4–8]. Snoeck et al. [9] used pneumatically driven harvesting finger rows to facilitate the shedding of coffee fruit from branches. Tascón et al. [10] used a vibrational harvesting method that involved clamping the main trunk and directly applying vibrations to the main trunk to facilitate the shedding of coffee fruit; however, this method is energy-intensive and causes considerable damage to the trunk. Cárdenas et al. [11] designed a harvesting device with a motor-driven three-tooth blade agitator; the device is lighter and more portable and has higher harvesting efficiency than manual harvesting by 70%, and its green harvest rate is approximately 4.5%. However, the harvesting efficiency of the device is considerably

low, with speed lower than that of manual operation. The Colombian National Research Center (Cenicafé) introduced the DSC-18 coffee harvesting machine, which produces high-frequency, low-amplitude vibrations with a short picking time and a harvest rate higher than 50% [12]; however, the machine has a high green harvest rate and generates a considerable amount of noise.

Few studies have focused on the coffee harvesting technology and machinery used in China. Yu et al. [13] designed a vibrating comb-type small-grain coffee harvesting device; however, the large working parts of the device cause damage to branches and leaves. Zong et al. [14] designed a beat-type chestnut harvesting device with high harvesting efficiency; however, the device has large working parts that cause considerable damage to the fruit and cannot be used for coffee harvesting. Wu et al. [15] analyzed the operation of a branch shaking-type oil-tea fruit harvesting device and investigated the main factors that influence the shedding of fruit during vibrational harvesting. Pneumatic harvesting methods are primarily used to harvest large forest fruits, such as citrus; but such methods require considerable amounts of energy and incur high costs. In the impact harvesting method, force is directly applied to the trunk and may cause external and internal damage to the tree [16–24]. By contrast, vibrational harvesting machinery causes less damage because it does not have direct contact with the fruit [25,26].

The present study aims to address the difficulty of mechanized harvesting of *Coffea arabica* L. in the mountainous areas of Yunnan Province because of the limited operating space. A handheld, lightweight, and easy-to-operate vibration-based coffee harvesting device was designed for the effective mechanized harvesting of *Coffea arabica* L. in Yunnan Province. In addition, this study established a model representing the vibration of coffee branches with fruit and identified the main factors that affect the shedding of the coffee fruit. The working parameter range of the proposed harvesting device was determined by establishing a “branch-mechanical” rigid-flexible coupling model and using the multi-body CAE software RecruDyn for simulations. Through field experiments, the optimal working parameters were determined for the vibrational harvesting of *Coffea arabica* L. in Yunnan Province, China. Thus, the study fills gaps in the literature on vibration-based mechanized harvesting of *Coffea arabica* L. in China and provides a theoretical basis for mechanized coffee harvesting.

## 2. Structure, Working Principle, and Design

### 2.1. Structure and Working Principle

Figure 1 illustrates the overall structure of the proposed coffee harvesting device. The device is composed of a motor, a crankshaft, a slider, a connecting rod, a spindle, a harvesting rod, an end cap, a bushing, an oil filling plug, a coupling, and a housing.

The device is held using the housing handle. When the harvester is switched on, the motor drives the crankshaft to rotate, causing an upward–downward motion in the slider along the groove at the end of the connecting rod. The connected rod swings left and right, driving the harvesting rod to swing left and right. When the branches of the small-grain coffee tree are placed between the V-shaped harvesting rod, they undergo vibrations of a certain amplitude and frequency because of the action of the harvesting rod. Harvesting is accomplished when the fruit detaches from the stalk under the action of a vibrational force greater than the inertial force of the small-grain coffee fruit and the force between the fruit and the stalk.

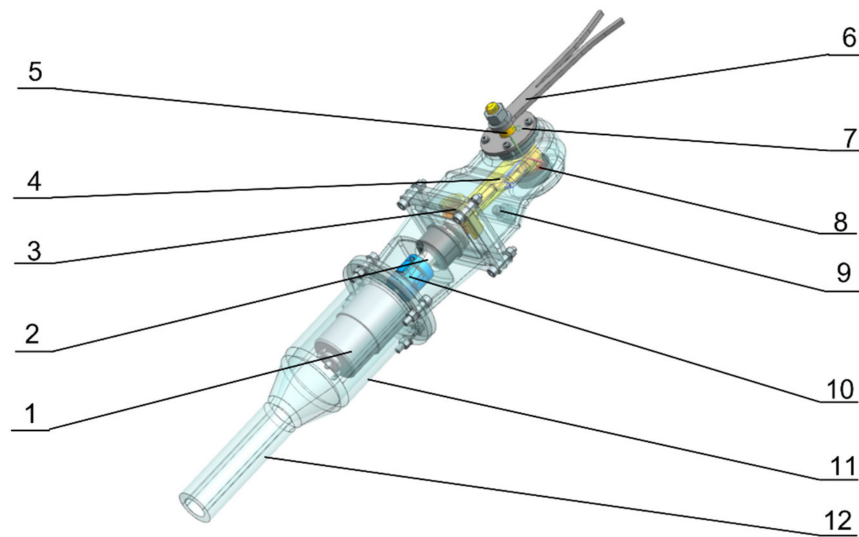


**Figure 1.** Schematic of the proposed handheld vibrating-type *Coffea arabica* L. harvester. 1—Motor; 2—Crankshaft; 3—Slider; 4—Connecting rod; 5—Spindle; 6—Harvesting rod; 7—End cap; 8—Bushing; 9—Oil filling plug; 10—Coupling; 11—Housing; and 12—Housing handle.

2.2. Design of the Crank-Slider Linkage Mechanism

The primary vibrating parts of the machine are the crank, slider, and end linkage (Figure 2), which operate through a single-degree-of-freedom space mechanism. During the operation of the machine, the crank drives the slider toward the slide groove. Then, the slider drives the harvesting rod through the driving linkage, thereby generating a simple harmonic motion that ensures the stability of the machine and helps accomplish harvesting.

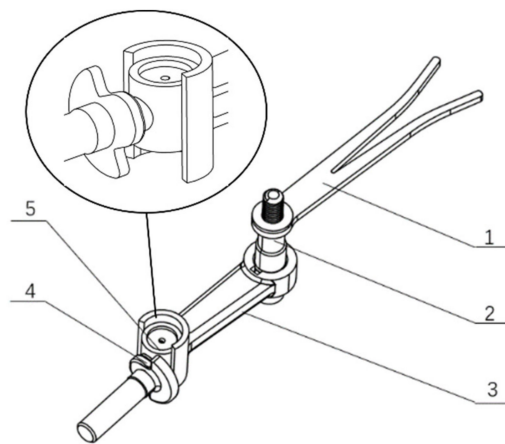


**Figure 2.** Schematic of the crank-rocker mechanism. 1—Harvesting rod; 2—Spindle; 3—Connecting rod; 4—Crank; 5—Slider.

The motion mechanism of the device is illustrated in Figure 3, where  $a$  denotes the crank eccentricity,  $b$  denotes the length of the connecting rod,  $c$  denotes the lowest clamping position of the harvest rod,  $d$  denotes the amplitude of the position,  $M$  and  $M'$  are the limits of the left–right moving crank’s position, and  $N$  and  $N'$  are the left and right limits of the clamping position, which can be derived using the theorem for similar triangles.

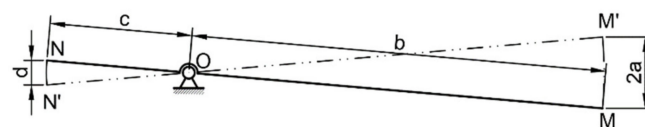


**Figure 3.** Schematic of the motion mechanism.

According to the preliminary results of the study, a vibration amplitude greater than 4 mm can achieve effective harvesting. Therefore, the minimum amplitude of the machine was fixed at 4 mm. Regarding the machine shell size, the clamping position of the harvesting rod position ( $c$ ) should be  $\geq 24$  mm from the spindle, considering that the machine is handheld. Furthermore, the proposed device achieved energy savings. In addition to minimizing device size, the stability of the machine was achieved by fixing the connecting rod length ( $b$ ) at 70 mm; the crank eccentricity ( $a$ ) was calculated to be 6 mm by using Equation (1):

$$\frac{2a}{d} = \frac{b}{c} \quad (1)$$

### 2.3. Design of the Harvesting Rod

The harvesting rod is in direct contact with the coffee branches during mechanized harvesting and thus directly affects harvesting efficiency and the degree of damage to the coffee branches. The diameters of the bottom, middle, and end sections of a mature coffee-tree branch are 6.3–7.5 mm, 5.8–6.2 mm, and 3.5–4.3 mm, respectively. The harvesting rod in the proposed device is V-shaped, with an opening range of 3.5–10 mm, to restrict the scattering of the coffee branch and minimize energy loss when the harvesting rod acts on the branch. Such a design also ensures that the harvesting rod is clamped to the branch when working.

The amplitude and frequency of the vibration were fixed at 6 mm and 60 Hz, respectively, for harvesting tests to limit the damage caused by the harvesting rod to the branches. At equal vibration frequencies, amplitudes, and excitation positions, three materials, namely acrylonitrile butadiene styrene (ABS), stainless steel, and aluminum, were used for harvesting coffee branches of comparable growth, and each set of tests was repeated thrice. The properties of the three materials are summarized in Table 1. The mature fruit picking rate, green fruit picking rate, and damage rate using each material were evaluated. The results indicated that the mature and green fruit picking rate using the three materials were identical, and the rate of damage caused by the ABS cloth to the branches was lower than that by stainless steel and aluminum. Therefore, ABS fabric was selected as the material for the harvesting rod.

**Table 1.** Properties of different materials.

Material	Stainless Steel	Aluminum	ABS
Elastic modulus E/MPa	$2.07 \times 10^5$	$7.2 \times 10^4$	200

## 3. Mechanical Analysis of Fruit Abscission

### 3.1. Analysis of Coffee Fruit-Stalk Separation Process through High-Speed Photography

A fruit-stalk vibration separation test was conducted using a high-speed camera at the Pu'er coffee plantation of Yunnan Agricultural University to analyze the principle of coffee fruit shedding by forced vibration. A vibrating coffee harvesting prototype was used to vibrate the branches with vibration amplitudes of 4, 6, 8, and 10 mm for the test, and three sets of harvesting pretests were conducted at each of the four amplitudes with vibration frequencies of 30, 35, 40, 45, 50, 55, 60, 65, 70, 75, and 80 Hz. The ripening rate  $U$  was used as the evaluation index, calculated using the following equation:

$$U = \frac{C}{A} \times 100\% \quad (2)$$

where  $A$  denotes the total number of ripe fruits on the branch, and  $C$  denotes the number of ripe fruits picked.

For the statistical collation of the harvesting ripening rate under each condition, the average value of three trials was calculated. The effects of different amplitudes and frequencies on the harvesting rate were plotted (Figure 4) using Origin software. When the

frequency was 60 Hz, the net harvesting rates corresponding to amplitudes of 8 and 10 mm were greater than 95%, the ripe harvesting rates corresponding to the two amplitudes were similar, and the harvesting effects were similar. However, with the increase in amplitude, the damage to the branches increased. Therefore, the frequency of 60 Hz and the amplitude of 8 mm were selected for the remainder of the analysis.

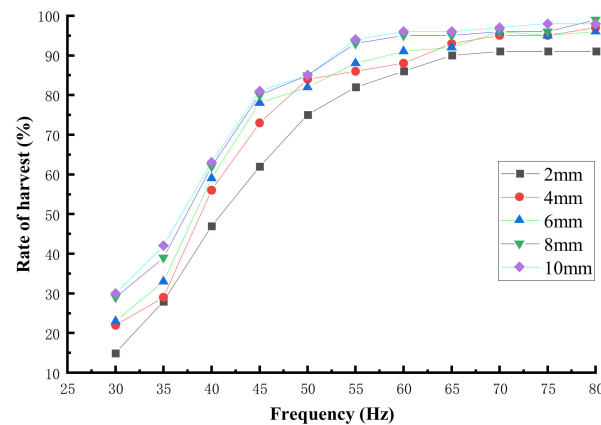


**Figure 4.** Effects of different amplitudes and frequencies on harvesting rate.

In the pretests, the vibration frequency and amplitude were 60 Hz and 8 mm, respectively. The center of the branch was the excitation position, and the vibration occurred in an upward–downward manner.

Tress of good growth and moderate maturity from the small-grain Katim variety were selected for the tests. After the surrounding excess branches and leaves were removed to prevent the formation of blind areas during vibration tracking, the coffee fruits were grouped and numbered, and the capture points were marked for subsequent tracking and analysis in VL3.0 software. After a certain period, the coffee fruit-stalk joint ruptured, and the coffee fruit detached from the stalk. A 5F01 Thousand-Eye Wolf high-speed camera was used to track and record the shedding of the coffee ripe fruit at a frame rate of 500 fps and a resolution of  $1280 \times 1024$  pixels, considering the lighting conditions and working environment of the test site. The test scene is illustrated in Figure 5.

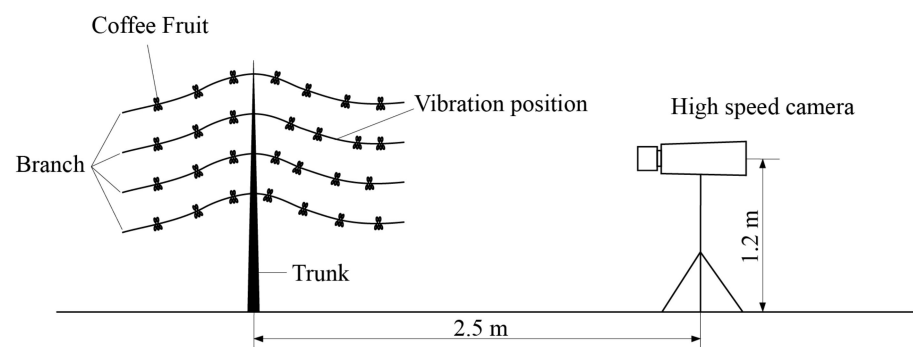


**Figure 5.** Schematic of high-speed photography.

The instantaneous velocity of the fruit was calculated through frame-by-frame tracking, and the non-essential data were eliminated. Then, the instantaneous velocity data for the separation process between the coffee fruit and the branch where it was located were compiled into five groups (the data for each group of 10 coffee fruits were averaged). Origin software was used to generate time-velocity curves of the moments of coffee fruit detachment, as illustrated in Figure 6, to determine the relative motion pattern between the coffee fruit and the branch.

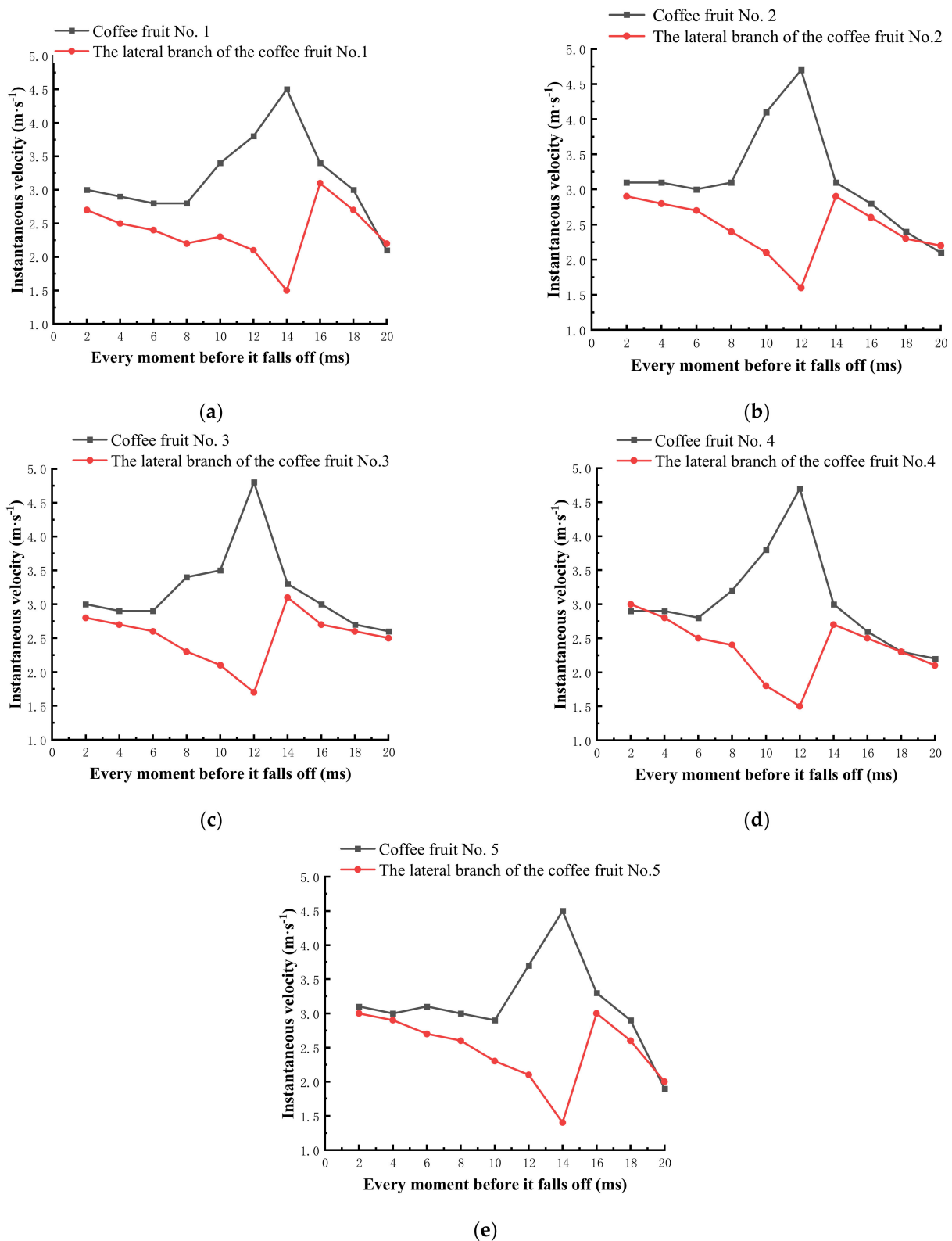


Figure 6. (a–e) Comparison of instantaneous velocities between five groups of the coffee fruit.

The overall pattern of changes in the instantaneous velocity of the separation process between the coffee fruit and the lateral branch where it was located was analyzed in three stages. Stage 1: the instantaneous velocity of both the coffee fruit and the lateral branch gradually increased 16–20 ms (coffee groups 1 and 5) or 14–20 ms (coffee groups 2, 3, and 4) before shedding on the horizontal plane; the relative instantaneous velocity was small, and

the relative motion was thus insignificant. Stage 2: the trends of the instantaneous velocities of the coffee fruit and its lateral branch were opposite 8–16 ms before abscission (coffee groups 1 and 5) or 6–14 ms before abscission (coffee groups 2, 3, and 4); the velocity of the coffee fruit first increased and then decreased, whereas the velocity of the lateral branch first decreased and then increased. The velocity of the coffee fruit was extremely high, and the relative instantaneous velocities of both the fruit and the branch were maximum. Stage 3: the changes in the cis-temporal velocities of both coffee fruit and its lateral branches were identical 2–8 ms before abscission (coffee groups 1 and 5) or 2–6 ms before abscission (coffee groups 2, 3, and 4).

The tests revealed two identical velocity trends and comparable in Stage 1, indicating that the coffee fruit-stalk joint had not ruptured in this stage. In Stage 2, when the fruit-stalk joint began to rupture, the two velocity trends changed, and the relative instantaneous velocity was maximum. In Stage 3, the two velocity trends were identical again, and the coffee fruit and the stalk gradually separated; the relative instantaneous velocities in this stage were higher than those in Stage 1.

The instantaneous velocity of each group of coffee fruit 20 ms before shedding was derived from the plot displayed in Figure 7. The movement trends of the coffee fruit in the first 20 ms before shedding were identical. In Stage 1, the coffee fruit exhibited accelerated movement along with the lateral branch. In Stage 2, the fruit velocity reached a peak value and then began to decrease, and the fruit-stalk joint began to rupture. In Stage 3, the coffee fruit exhibited a nearly uniform movement, with relative movement between the coffee fruit and the lateral branch that resulted in the detachment of the coffee fruit from the stalk.

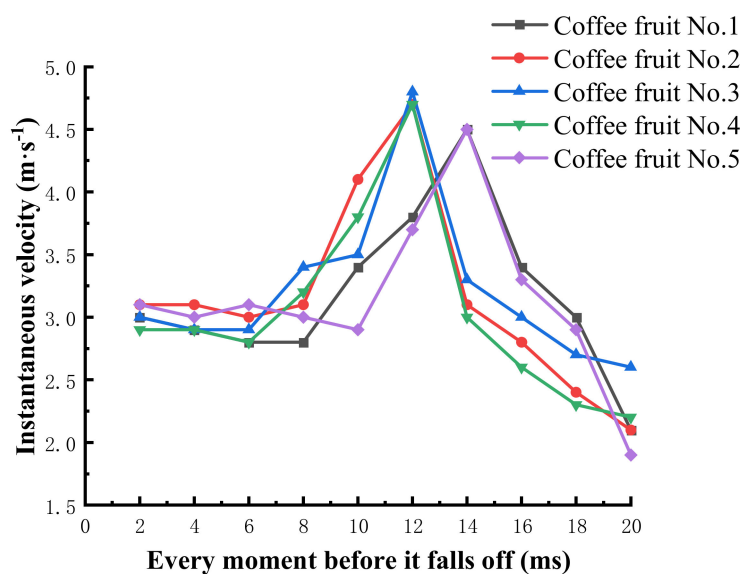
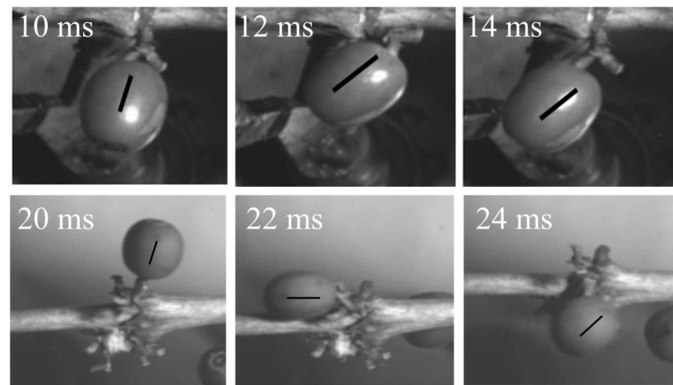


Figure 7. Changes in the instantaneous velocity of coffee fruit at each moment before shedding.

Figure 8 illustrates the motion of a coffee fruit at three instants with a spacing of 2 ms. The analysis revealed two states of the coffee fruit during the motion.

1. As displayed in the upper three diagrams in Figure 8, the coffee fruit exhibited reciprocal oscillation under the action of inertial forces, with the fruit-stalk joint as the center of rotation. The coffee fruit-stalk joint was influenced by a tangential force.
2. As displayed in the lower three diagrams in Figure 8, the coffee fruit exhibited a simple harmonic motion under the action of inertial forces, with the stalk-branch joint as the center of rotation and the length of the stalk as the radius of rotation. The coffee fruit-stalk joint was influenced by a normal force.



**Figure 8.** Movement pattern of the coffee fruit.

In summary, the coffee fruit and the lateral branch were in motion, and an inertial force was exerted on the coffee fruit-stalk connection during the motion. The fruit-stalk joint ruptured when the velocities of the coffee fruit and the lateral branch were maximum. Subsequently, the shedding of the coffee fruit occurred when the resultant of the tangential and normal forces acting on the coffee fruit was greater than the resultant of the force between the fruit and the stalk.

### 3.2. Kinetic Modeling and Analysis of Harvesting

#### 3.2.1. Mechanical Analysis of Coffee Fruit Abscission

The high-speed photographic analysis revealed that the coffee fruit was subjected to two forces, namely a normal inertial force and a tangential inertial force, when forced vibration was applied. For further analysis, the coffee fruit-stalk joint was simplified to a single pendulum model [27]. As illustrated in Figure 9, a fruit-stalk model coordinate system was established, with the fruit-stalk joint as the origin O, the vertical direction perpendicular to the branch axis as the  $y$ -axis, and the horizontal direction perpendicular to the branch axis as the  $x$ -axis.

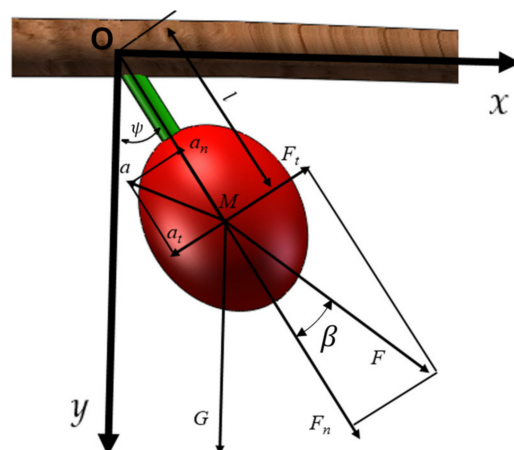


**Figure 9.** Inverse pendulum model of *Coffea arabica* L.

The normal inertial force  $F_n$  and the tangential inertial force  $F_t$  can be expressed as follows:

$$\begin{cases} F_n = ma_n = m \left( \frac{d\psi}{dt} \right)^2 l \\ F_t = ma_t = m \frac{d^2\psi}{dt^2} l \end{cases} \quad (3)$$

where  $a_n$  is the normal acceleration ( $\text{m}\cdot\text{s}^{-2}$ );  $a_t$  is the tangential acceleration ( $\text{m}\cdot\text{s}^{-2}$ );  $m$  is the small-grain coffee single fruit quality (kg);  $\psi$  is the angular displacement of coffee fruit rotation (rad); and  $l$  is the length of coffee branch nodes to the coffee fruit placenta (m).

The combined force  $F$  on the coffee fruit-stalk joint is expressed as follows:

$$F = \sqrt{F_n^2 + F_t^2} = \sqrt{(ml)^2 \left(\frac{d\psi}{dt}\right)^4 + \left(ml \frac{d^2\psi}{dt^2}\right)^2} \quad (4)$$

### 3.2.2. Dynamic Model of the Forced Vibration of Coffee Fruit

According to the force model of the coffee fruit and the kinetic energy theorem, the kinetic energy ( $T_D$ ) of the coffee fruit with respect to the branch was calculated using the following equation:

$$T_D = \frac{1}{2}m \left(l \frac{d\psi}{dt}\right)^2 + \frac{1}{2}I_c \left(\frac{d\psi}{dt}\right)^2 \quad (5)$$

where  $I_c$  denotes the coffee fruit rotational inertia ( $\text{kg}\cdot\text{m}^2$ );  $t$  denotes the time (s).

According to the force model of the coffee fruit and the potential energy theorem, the potential energy ( $V_D$ ) of the coffee fruit with respect to the branch was as follows:

$$V_D = \frac{1}{2}k(l\psi)^2 + mgl \cos \psi \quad (6)$$

where  $k$  denotes the equivalent elasticity coefficient of the coffee fruit-stalk joint;  $g$  denotes the gravitational acceleration ( $\text{m}/\text{s}^2$ ).

The Lagrangian quantity ( $L$ ) was calculated using the Lagrangian function [28] as follows:

$$L = T_D - V_D = \frac{1}{2}m \left(l \frac{d\psi}{dt}\right)^2 + \frac{1}{2}I_c \left(\frac{d\psi}{dt}\right)^2 - \left(\frac{1}{2}kl^2\psi^2 + mgl \cos \psi\right) \quad (7)$$

which can be expressed as the following Lagrange's equation [29]:

$$\frac{d}{dt} \left( \frac{\partial L}{\partial \dot{\psi}} \right) - \frac{\partial L}{\partial \psi} = 0 \quad (8)$$

The differential equation for the vibration of the coffee fruit was obtained by substituting values from Equation (7) into Equation (8):

$$\frac{d}{dt} \left( \frac{\partial L}{\partial \dot{\psi}} \right) - \frac{\partial L}{\partial \psi} = m \frac{d^2\psi}{dt^2} l + I_c \frac{d^2\psi}{dt^2} - kl^2\psi + mgl \sin \psi = 0 \quad (9)$$

### 3.2.3. Analysis of the Vibration System

A periodic external force  $F_0$  was applied to the branch:

$$F_0 = A \sin(\omega t) \quad (10)$$

where  $A$  denotes the amplitude of the force, and  $\omega$  denotes the applied frequency of the force.

A coordinate system was established with the direction of the excitation force as the  $y$ -axis and the vertical direction of the branch as the  $x$ -axis. The branch vibration generated by the inertial force can be expressed as follows:

$$F_1 = M_1 \frac{d^2y}{dt^2} \quad (11)$$

where  $M_1$  denotes the equivalent mass of the branch.

The elastic force  $f_k$  generated by the branch was:

$$f_k = k_1 y \quad (12)$$

where  $k_1$  is the elasticity coefficient of the branch.

The damping force  $f_c$  on the branch was:

$$f_c = c \frac{dy}{dt} \tag{13}$$

where  $c$  denotes the damping coefficient, and  $y$  denotes the displacement of the branch in the  $y$ -axis direction (m).

The instantaneous resultant of the inertial force, damping force, elastic force, and external force during vibration was equal to 0, as expressed by the following equation:

$$-F_0 + M_1 \frac{d^2y}{dt^2} + k_1y + c \frac{dy}{dt} = 0 \tag{14}$$

Equation (14) can be expressed in the general form of the vibration differential equation as follows:

$$M_1 \frac{d^2y}{dt^2} + k_1y + c \frac{dy}{dt} = F_0 \tag{15}$$

The maximum displacement ( $S$ ) of the branch off-center was

$$S = \frac{A}{\sqrt{(k_1 - M_1\omega^2)^2 + c\omega^2}} \tag{16}$$

The vibration displacement ( $y$ ) of the branch in the  $y$ -direction can be expressed as follows:

$$y = S \sin \omega t \tag{17}$$

Because the displacement of the branch in the  $x$ -direction was considerably small under practical conditions, only the motion in the  $y$ -direction was considered to simplify the proposed motion model.

When the coffee branch was forced to vibrate, the relative motion of the fruit and the branch was neglected, and the motion law of the branch was identical to that of the coffee fruit [30]. The vibration displacement of the coffee branch can be expressed as follows:

$$y_1 = S \sin \omega t \tag{18}$$

Considering that the motion of all coffee fruits on a branch was identical and that the relative motion of the branch and coffee fruits was not negligible, the total energy of the coffee branch was calculated according to the kinetic energy theorem as follows:

$$E = E_F - E_K - E_C = \frac{1}{2}M_1\left(\frac{dy}{dt}\right)^2 + \frac{1}{2}m_1\left(\frac{dy_1}{dt}\right)^2 + \frac{1}{2}m_1\left(l\frac{d\psi}{dt}\right)^2 + \frac{1}{2}I_c\left(\frac{d\psi}{dt}\right)^2 \tag{19}$$

where  $m_1$  denotes the total mass of coffee fruits on the branch;  $E_F$  denotes the output energy of the excitation force ( $J$ );  $E_K$  denotes the energy consumed by the elastic force ( $J$ ); and  $E_C$  denotes the energy consumed by the damping force ( $J$ ).

Substituting Equations (16)–(18) into (19):

$$\frac{d\psi}{dt} = \sqrt{\frac{2[(k_1 - M_1\omega^2)^2 + (c\omega^2)](E_F - E_K - E_C) - (M_1 + m_1)(A \cos \omega t)^2}{(m_1l^2 + I_c)[(k - M_1\omega^2)^2 + (c\omega^2)]]} \tag{20}$$

Therefore,  $[(k - M_1\omega^2)^2 + (c\omega^2)] = P$ ,  $M_1 + m_1 = M$ , and  $m_1l^2 + I_c = N$ . The derivative of Equation (20) was as follows:

$$\frac{d^2\psi}{dt^2} = \frac{MA^2(\cos \omega t)(\sin \omega t)}{\sqrt{[2PE - M(A \cos \omega t)^2]NP}} \tag{21}$$

With the increase in the resultant force on the coffee, the fruit was shed more readily. According to Equations (4), (20), and (21), the resultant force on the coffee fruit during the movement was

$$\begin{aligned}
 F &= \sqrt{F_n^2 + F_t^2} = \sqrt{(ml)^2 \left(\frac{d\psi}{dt}\right)^4 + (ml \frac{d^2\psi}{dt^2})^2} \\
 &= \sqrt{\frac{m^2 l^2 [2PE - M(A \cos \omega t)^2]^2}{N^2 P^2} + \frac{m^2 l^2 M^2 A^4 (\cos \omega t)^2 (\sin \omega t)^2}{[2PE - M(A \cos \omega t)^2] NP}}
 \end{aligned}
 \tag{22}$$

The inertial force on the coffee fruit increased with the amplitude and frequency of the excitation force, thus facilitating the shedding of the fruit. Furthermore, when the location of the excitation force was closer to the coffee fruit, less energy was consumed by the elastic force ( $E_K$ ) and the damping force ( $E_C$ ); therefore, both  $E$  and  $F$  increased, and the coffee fruit shed more readily. Moreover, the greater the energy output ( $E_F$ ) of the excitation force ( $E$ ) and the resultant force acting on the coffee fruit increased with the length of the excitation branch, thereby facilitating the shedding of the coffee fruit. However, excessive vibration frequency and vibration amplitude on the branch can cause damage to the branch, and the overall harvesting effect may be different at different excitation positions. Thus, the appropriate frequency, amplitude, and excitation position should be determined.

#### 4. Modeling and RecurDyn Simulation

##### 4.1. Fruit-Bearing Branch Modeling

To establish an accurate fruit tree model, the physical and mechanical characteristics of 4 year old small-grain coffee trees of the Katim variety were obtained using a digital display push-pull meter (SF-20) at the coffee plantation of the College of Tropical Crops, Yunnan Agricultural University, Pu'er City, Yunnan Province. The fruit-stalk bond was measured using a digital display push-pull meter (SF-20) in the direction of the fruit stalk, as illustrated in Figure 10. A total of 50 sets of samples were selected from each of the ripe and unripe fruits, and the results of the measurements are listed in Table 2. The branch length, node spacing, and branch diameter of the coffee trees were measured using a measuring tape and vernier caliper; the results are listed in Table 3. The samples were collected, and the density and elastic modulus of small coffee fruits were measured using a mass spectrometer (TA Type-XTPlus), high-precision electronic scale (JA5103 with an accuracy of 0.001 g), and measuring cylinder; the results are listed in Table 4.



Figure 10. Tensile test using a digital push-pull meter.

Table 2. Binding capacity ranges of coffee fruit with different maturity levels.

Name	Range
Binding force between green fruit and fruit handle (N)	9.89–11.92
Binding force between mature fruit and fruit handle (N)	3.56–5.82

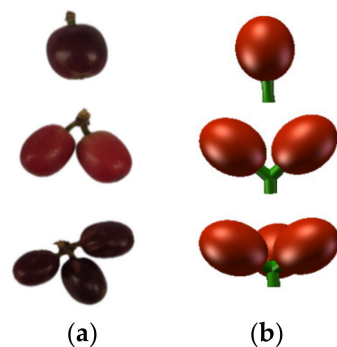
**Table 3.** Tree shape parameters of *Coffea arabica* L.

Name	Mean Value	Standard Deviation
Front diameter of coffee fruit branch (mm)	6.9	0.49
Middle diameter of coffee fruit branch (mm)	6.0	0.42
Rear segment diameter of coffee fruit branch (mm)	4.2	0.45
Diameter of coffee fruit branch (mm)	487.8	12.59
Number of nodes on coffee branches	11.8	2.31
Number of coffees per node	9.2	3.85
Average node spacing (mm)	48	0.52
Length of fruit stem (mm)	3.66	0.33
Diameter of fruit stem (mm)	1.71	0.28
Density of fruit stem (g/cm <sup>3</sup> )	1.18	0.16
Density of branch (g/cm <sup>3</sup> )	0.76	0.21
Elastic modulus of fruit stem (MPa)	1860	0.43
Elastic modulus of the branch (MPa)	2861.2	0.46

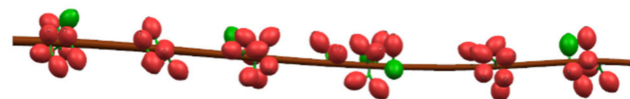
**Table 4.** Physical and mechanical properties of the coffee fruit and stem.

		Length (mm)	Diameter (mm)	Density (g/cm <sup>3</sup> )	Elastic Modulus (MPa)	Poisson's Ratio
Coffee fruit	Green	16.1	12.7	0.93	15.82	0.24
	Mature	17.1	14.8	0.97	2.93	0.28
Stem	Green	6.64	2.12	0.80	15.74	0.35
	Mature	6.36	2.32	0.86	23.9	0.35

Coffee fruits are distributed in clusters on the nodes of branches. According to the actual growth characteristics of fruits and stalks, a 3D digital model (Figure 11) of the coffee fruit-stalk joint was established through NX12.0 random modeling.

**Figure 11.** Model of the coffee fruit-stalk joint. (a) Image of the coffee fruit (b) 3D model of the coffee berry.

Based on the data in Tables 3 and 4, the coffee branch was modeled using NX12.0. Because the coffee branch is a flexible body, the coffee branch model was discretized, and the coffee fruit-stalk model was assembled with the branch model to obtain a coffee branch model with fruit, as displayed in Figure 12.

**Figure 12.** Modeling of a coffee stick.

#### 4.2. Simulation of Rigid Body and Multi-Flexible Body Coupling

The obtained model of the branch with fruit was converted to the step format and imported into Hypermesh software for geometric model processing, meshing, and material assignment. Hexahedral meshing was selected for division in Hypermesh to reduce the overall computational effort of the simulation [31]. The divided mesh file was imported into

RecurDyn in the bdf format to generate a flexible branch body. Then, the machine model was simplified and converted to the step format and imported into RecurDyn software, and the coffee branch flexible body model was assembled with the simplified machine model to derive a branch-machine coupling model, as illustrated in Figure 13.

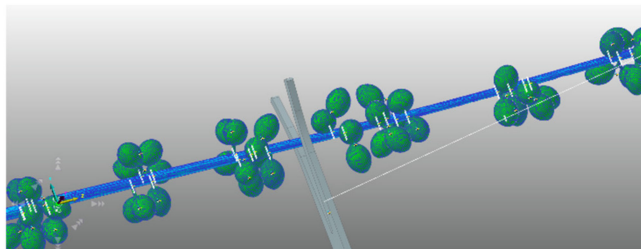


**Figure 13.** Rigid–flexible branch-machine coupling model.

A driving force was applied to a rotation sub added to the harvesting rod, and the motion of the harvesting rod was set to reciprocal periodic rotation motion. The coffee branch was simulated as a cantilever beam model with the bottom end as the fixed end and the other end as the free end. Some constraints were fixed, and a GeoSurface contact was established between the pendulum and the flexible coffee branch. Bushing constraints were added between the branch and the fruit stalk, and between the fruit stalk and the fruit. Markers were added to the finite element nodes before exporting acceleration to the flexible editing interface, and before exporting the acceleration of each coffee fruit center of mass. The magnitude of the inertial force on the coffee fruit was calculated using the acceleration and fruit mass. When the force was greater than 5.82 N, the coffee fruit was considered shed, and the number of the shed coffee berries was recorded.

#### 4.3. Single-Factor Simulation Test

Frequency, amplitude, and excitation position were selected as the test factors to determine their influence on coffee fruit shedding; the number of shed coffee berries was selected as the test index for the one-way simulation test. The excitation position was expressed as the ratio between the length of the action point from the branch to the trunk and the total length of the branch. In the pretests, the fixed values of each test factor were 55 Hz, 6 mm, and 0.5 L, respectively. The frequency range was varied from 10 to 90 Hz, the amplitude ranged from 2 to 12 mm, and the excitation position ranged from 0.1 to 0.9 L.

##### 4.3.1. Effects of Different Frequencies on Fruit Abscission

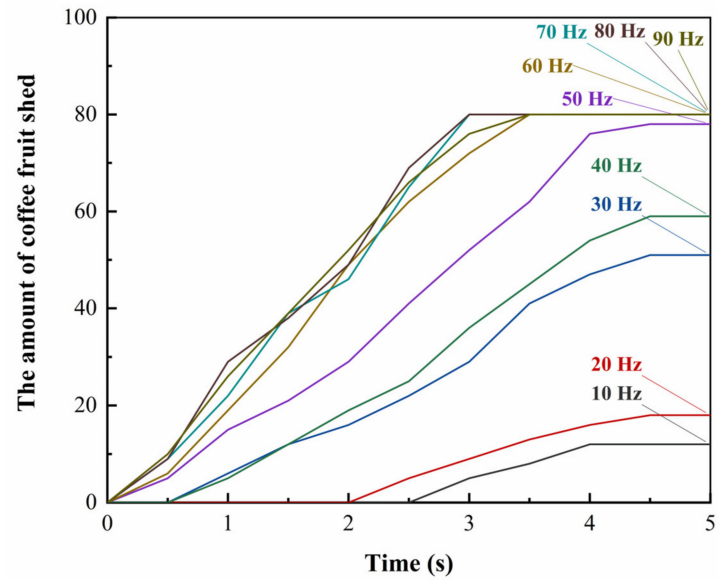
The number of fallen fruits increased with the increase in frequency (Figure 14a) because the inertial force acting on the coffee fruit increased with the frequency, thereby facilitating the shedding of the coffee fruit. When the frequency was lower than 30 Hz, the shedding of the coffee fruit was gradual, and the harvesting efficiency was thus low. When the frequency reached 50 Hz, the harvesting effect improved. Furthermore, the amount of coffee fruit shed at a frequency of 90 Hz was the same as that at a frequency was 80 Hz. Therefore, the frequency range of 40–80 Hz was selected for the proposed device.

##### 4.3.2. Effects of Different Amplitudes on Fruit Abscission

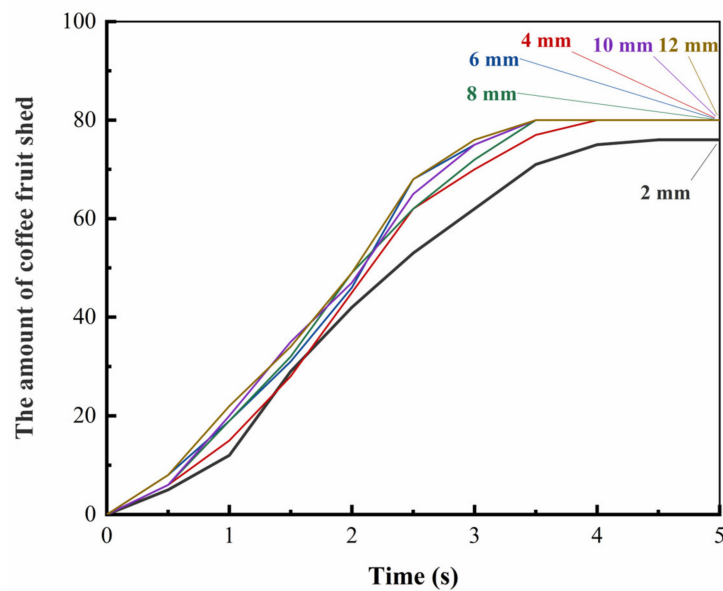
The number of fallen fruits increased with the increase in amplitude (Figure 14b) because the inertial force on the coffee fruit increased with the amplitude, thereby facilitating the shedding of the coffee fruit. When the amplitude was lower than 4 mm, the coffee shedding was more gradual; when the amplitude was higher than 12 mm, the harvesting effect was satisfactory. Therefore, the amplitude range of 4–12 mm was selected for the proposed device.

### 4.3.3. Effects of Different Excitation Positions on Fruit Abscission

When the excitation position was 0.5 L, the harvesting effect of the device was the most pronounced (Figure 14c) and optimal. However, the harvesting effect decreased on the two sides of the excitation position in the middle because the energy transferred to the two sides of the branch was the lowest.



(a)



(b)

Figure 14. Cont.

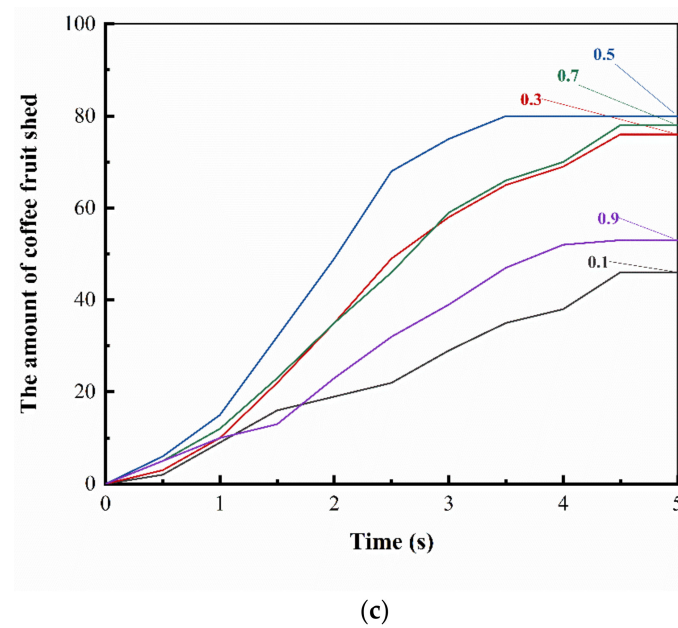


**Figure 14.** Effects of different factors on the shedding process: (a) effects of different frequencies on fruit abscission, (b) effects of different amplitudes on fruit abscission, and (c) effects of different excitation positions on fruit abscission.

## 5. Experiments

A prototype of the proposed harvesting device was developed at the Engineering Training Center of Kunming University of Science and Technology to analyze the effects of vibration frequency, amplitude, and excitation position on coffee ripening rate, harvesting rate, and fruit damage rate, and to further determine the range of vibration parameters. Furthermore, a small-grain coffee vibrational harvesting test was conducted at the coffee cultivation base of the Pu'er Campus of Yunnan Agricultural University.

The test was conducted on 20 December 2021. The meteorological data for the test day are listed in Table 5, and the actual photograph of the base is displayed in Figure 15.

**Table 5.** Meteorological data.

Meteorological Type		Meteorological Type	
Altitude	1050 m	Relative humidity	76.4%
Average temperature	16 °C	Wind speed	0.6 m/s
Temperature difference	12 °C	Hydrothermal coefficient	1.652



**Figure 15.** Test site.

The equipment and tools used in the test included a sample harvesting machine, digital vernier caliper, toolbox, measuring tape, Kestrel3500 portable weather station, tachymeter, and fruit catching bag.

#### Test Program

Through the aforementioned analysis, the vibration frequency, the vibration amplitude, and the excitation position of the harvesting rod were determined as the test factors. The vibration frequency of the harvesting rod was varied by controlling the motor speed, and the vibration amplitude was varied by replacing the harvesting rod at different clamping positions. The test used the ripe fruit picking rate ( $U$ ), unripe fruit picking rate ( $V$ ), and coffee fruit damage rate ( $W$ ) as the comprehensive evaluation indexes. The following equations were used for calculations:

$$U = \frac{C}{A} \times 100\% \quad (23)$$

$$V = \frac{B}{D} \times 100\% \quad (24)$$

$$W = \frac{H}{G} \times 100\% \quad (25)$$

where  $A$  denotes the number of ripe fruit on the branch;  $B$  denotes the number of immature fruit picked;  $C$  denotes the number of ripe fruit picked;  $D$  denotes the number of immature fruit on the branch;  $H$  denotes the number of coffee fruit damage;  $G$  denotes the total number of coffee fruit picked. Fruit damage was assessed by determining whether the peel of the picked coffee fruit and the fruit-stalk joint were damaged.

Before the test, the amplitude of the harvesting rod was first varied, and the coffee branches of similar length were selected as the test objects to reduce errors in the calculation of the test index. The circuit control was switched on, the desired motor speed was selected, the harvesting rod was clamped to the branch, the branch was vibrated for 5 s, and experimental data were recorded. The harvesting process and harvested berries are illustrated in Figure 16.

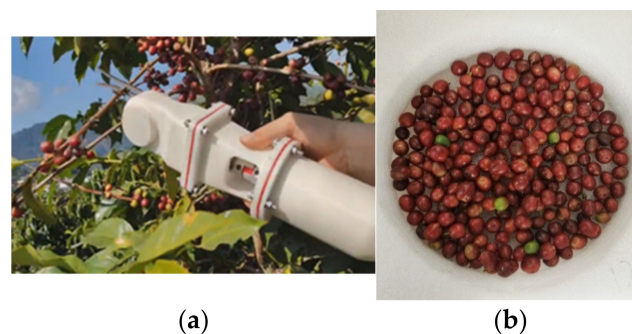


**Figure 16.** Test process and results: (a) harvesting process, and (b) harvested fruit.

A central composite design was adopted for a three-factor five-level quadratic orthogonal rotational combination test [32]. The test factors and levels were coded as illustrated in Table 6. The experiment was conducted in 23 groups, with each group of experiments triplicated and their results averaged. Table 7 presents a summary of the experimental design scheme and results;  $Y_1$ ,  $Y_2$ , and  $Y_3$  in the table denote the ripe harvesting rate, harvesting growth rate, and fruit damage rate, respectively. The results of the analysis of variance (ANOVA) are displayed in Table 8.

**Table 6.** Codes of factors.

Level Codes	Test Factors		
	Frequency $X_1$ (Hz)	Amplitude $X_2$ (mm)	Excitation Position $X_3$
−1.682	40	4	0.2
−1	46	5.6	0.3
0	60	8	0.5
1	74	10.4	0.6
1.682	80	12	0.8

**Table 7.** Test design scheme and test results.

Test No.	Test Factors			Experimental Index		
	$X_1$	$X_2$	$X_3$	$Y_1$ (%)	$Y_2$ (%)	$Y_3$ (%)
1	−1	−1	−1	64.21	6.76	4.86
2	1	−1	−1	67.98	8.89	5.79
3	−1	1	−1	72.45	7.26	5.88
4	1	1	−1	82.45	8.96	6.75
5	−1	−1	1	83.12	8.16	5.14
6	1	−1	1	78.59	14.16	10.12
7	−1	1	1	72.02	10.36	5.89
8	1	1	1	98.33	18.36	12.26
9	−1.682	0	0	62.23	6.81	4.46
10	1.682	0	0	92.55	16.78	7.45
11	0	−1.682	0	71.21	8.97	4.23
12	0	1.682	0	89.79	13.61	6.41
13	0	0	−1.682	77.42	7.01	3.58
14	0	0	1.682	91.87	12.75	7.28
15	0	0	0	93.04	8.58	5.64
16	0	0	0	89.24	11.72	5.91
17	0	0	0	84.12	8.94	4.49
18	0	0	0	91.63	8.82	5.43
19	0	0	0	91.71	7.15	5.96
20	0	0	0	90.12	10.41	5.37
21	0	0	0	95.12	11.67	4.38
22	0	0	0	88.53	9.89	6.86
23	0	0	0	93.25	10.69	6.17

**Table 8.** Results of ANOVA.

Source of Variance	Mature Fruit Picking Rate				Green Fruit Picking Rate				Damage Rate			
	SS	df	F	p	SS	Df	F	p	SS	df	F	p
SS <sub>R</sub>	2232.91	9	12.02	<0.0001 **	189.57	9	10.82	0.0001 **	66.03	9	6.63	0.0013 **
$X_1$	546.66	1	26.49	0.0002 **	87.53	1	44.97	<0.0001 **	24.26	1	21.93	0.0004 **
$X_2$	286.48	1	13.88	0.0025 **	15.95	1	8.19	0.0133 *	5.33	1	4.82	0.0468 *
$X_3$	351.37	1	17.03	0.0012 **	60.83	1	31.25	<0.0001 **	19.58	1	17.70	0.0010 **
$X_1 X_2$	171.77	1	8.32	0.0128 *	0.31	1	0.16	0.6972	0.22	1	0.20	0.6622
$X_1 X_3$	8.02	1	0.39	0.5438	12.93	1	6.64	0.0230 *	11.40	1	10.31	0.0068 **
$X_2 X_3$	24.75	1	1.20	0.2933	4.25	1	2.18	0.1634	0.10	1	0.094	0.7645
$X_1^2$	447.86	1	21.71	0.0004 **	5.15	1	2.65	0.1278	3.25	1	2.94	0.1100
$X_2^2$	281.00	1	13.62	0.0027 **	2.42	1	1.24	0.2852	0.82	1	0.74	0.4048
$X_3^2$	117.06	1	5.67	0.0332 *	0.18	1	0.094	0.7640	1.07	1	0.97	0.3428
Residual	268.23	13			25.30	13			14.38	13		
Lack of fit	184.39	5	3.52	0.0561	6.75	5	0.58	0.7144	9.44	5	3.06	0.0777
Pure error	83.85	8			18.55	8			4.94	8		
Total variance	2501.14	22			214.87	22			80.41	22		

Note: \* indicates statistical significance ( $0.01 < p < 0.05$ ), \*\* indicates extremely high significance ( $p < 0.01$ ).

**6. Results**

As depicted in Table 8, the statistical significance of the regression model was  $<0.05$  for the ripening rate and  $0.0561 (>0.05)$  for the misfit term, indicating that the results obtained using the model were statistically significant and that the equation fit well. After the nonsignificant factors ( $p > 0.05$ ) were eliminated from the regression model, the following regression equation of the ripening rate was obtained:

$$Y_1 = 90.82 + 6.35X_1 + 4.60X_2 + 5.07X_3 + 4.63X_1X_2 - 5.39X_1^2 - 4.27X_2^2 - 2.71X_3^2 \quad (26)$$

The influence of all the factors, including frequency, excitation position, and amplitude, on the ripening rate and the interaction between frequency and amplitude were considered. The corresponding response surfaces are displayed in Figure 17a. When the excitation

position was 0.5 L, the ripening rate increased with the increase in the frequency and amplitude, and the growth rate of ripening decreased slightly with the increase in the frequency and amplitude.

The  $p$  value of the regression model was  $<0.05$  for the harvesting rate and  $0.7144$  ( $>0.05$ ) for the misfit term, indicating that the results obtained using the model were statistically significant and that the equation fits well. After the nonsignificant factors ( $p > 0.05$ ) were eliminated from the regression model, the following regression equation of the harvesting rate was obtained:

$$Y_2 = 9.78 + 2.54X_1 + 1.08X_2 + 2.11X_3 + 1.27X_1X_3 \quad (27)$$

The influence of all factors, including frequency, excitation position, and amplitude, on the extraction rate and the interaction between frequency and excitation position should be considered. The corresponding response surfaces are displayed in Figure 17b. When the amplitude was 8 mm, the extraction rate gradually increased with the increase in the frequency and excitation position, and the rate of increase in the extraction rate continued to increase.

The  $p$  value of the regression model for injury rate was  $<0.05$  and  $0.0777$  ( $>0.05$ ) for the misfit term, indicating that the results obtained using the model were statistically significant and that the equation fit well. After the nonsignificant factors ( $p > 0.05$ ) were eliminated from the regression model, the following regression equation for the injury rate was obtained:

$$Y_3 = 5.54 + 1.34X_1 + 0.63X_2 + 1.20X_3 + 1.19X_1X_3 \quad (28)$$

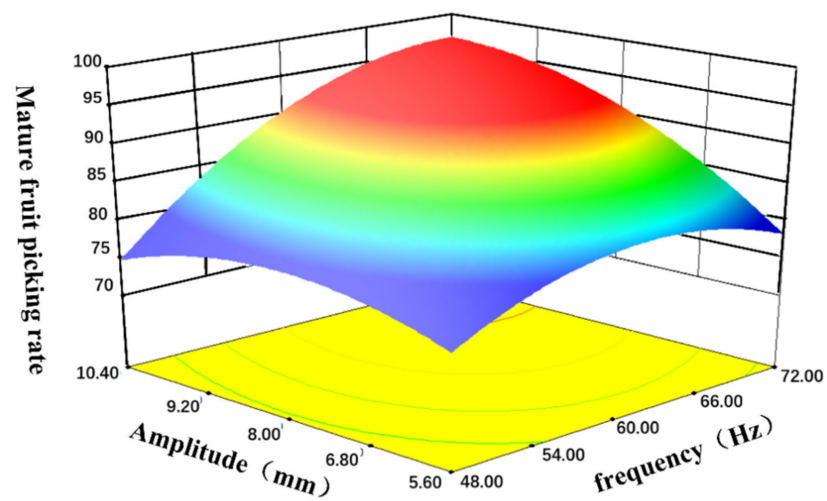
The influence of all the factors, including vibration frequency, excitation position, and amplitude, on the fruit damage rate and the interaction between frequency and excitation position were evaluated. The corresponding response surfaces are displayed in Figure 17c. When the amplitude was 8 mm, the damage rate gradually increased with the increase in the frequency and excitation position, and the rate of increase continued to increase.

The maximum recovery rate, minimum recovery rate, and damage rate were selected, and certain conditions of each factor were combined to achieve a recovery rate higher than 90%, recovery rate less than 10%, and damage rate less than 10%; the test indexes were optimized.

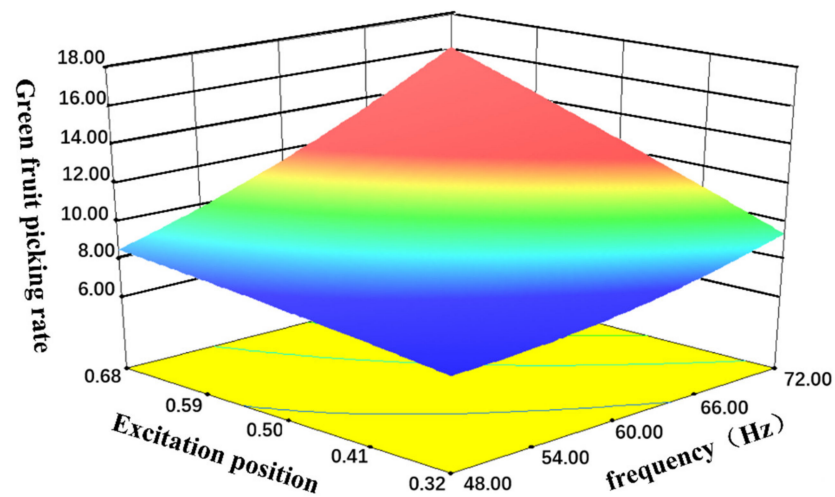
$$\left\{ \begin{array}{l} \max Y_1 \\ \min Y_2 \\ \min Y_3 \\ 40 \text{ Hz} \leq X_1 \leq 80 \text{ Hz} \\ 4 \text{ mm} \leq X_2 \leq 12 \text{ mm} \\ 0.1 \text{ L} \leq X_3 \leq 0.9 \text{ L} \end{array} \right. \quad (29)$$

The highest rate of ripening and the lowest rates of recovery and damage at a vibration frequency of 62 Hz, a vibration amplitude of 9 mm, and an excitation position of 0.4 L were calculated. The obtained values were 90.88%, 9.64%, and 5.52%, respectively.

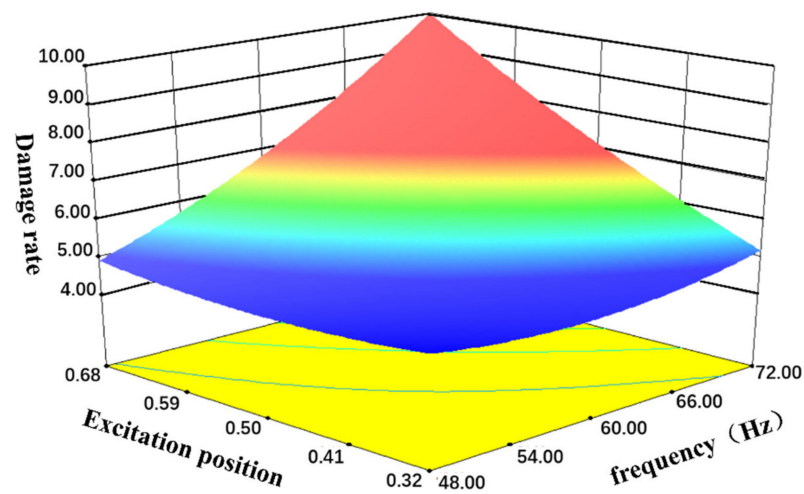
The reliability of the optimization results was verified by selecting 10 coffee trees with similar growth. The machine's vibration frequency, amplitude, and excitation position were fixed at 62 Hz, 9 mm, and 0.4 L, respectively, for 10 harvesting tests. Each test involved harvesting one tree, and the data for all 10 tests were recorded. The results indicated that the average mature fruit picking rate, green fruit picking rate, and damage rate for the 10 trials were 92.22%, 8.33%, and 5.23%, respectively. This indicated the validity of the optimization results.



(a)



(b)



(c)

**Figure 17.** (a) Response surfaces of the interaction between amplitude and frequency of the active branch; (b) response surfaces of the interaction between excitation position and frequency of the active branch; (c) response surfaces of the interaction between excitation position and frequency of the active branch.

## 7. Discussion

*Coffea arabica* L. cultivation in China is primarily concentrated in Yunnan Province, where the terrain is predominantly hilly and mountainous. A highly intensive planting method is required for cultivating *Coffea arabica* L., which cannot be harvested directly using large self-propelled harvesting machinery. In addition, manually carrying heavy machinery uphill is challenging because of the steep slopes and small planting terraces of Yunnan Province, limiting the development of the coffee industry in China.

Cárdenas et al. designed a harvesting device with a motor-driven three-tooth blade agitator, which has higher harvesting efficiency than traditional manual harvesting by 70% [11]. Snoeck et al. proposed a harvesting comb in direct contact with the coffee fruit, but it causes both ripe and unripe fruit to shed, resulting in coffee fruit waste [9]. Tascón et al. designed a portable long-pole picking device for harvesting fruit from high-density coffee plantations in Colombia. This device can work on slopes with a depth of 1.2 m and a gradient of 50°, and has harvesting efficiencies of 53–67 kg/h, which are considerably higher than that of conventional manual harvesting methods (12 kg/h) by 341.7–458.3% [4]. However, carrying this device to hilly planting environments is challenging because it is relatively heavy, thereby increasing farmers' workload.

In this study, a lightweight and easy-to-operate harvesting device was designed. Using a vibrational harvesting model and through rigid-flexible coupling simulations, vibration frequency, vibration amplitude, and excitation position, along with their specific ranges, were determined as the three main factors affecting the harvesting of *Coffea arabica* L. The optimal parameter combination was determined through field tests in a coffee plantation in Pu'er City, Yunnan Province. The results indicated that the efficiency of manual coffee harvesting by local farmers was 10 kg/h, but while using the proposed machine, the efficiency could reach 70–75 kg/h, increasing the harvesting efficiency of *Coffea arabica* L. by 700–750%. The ripe fruit harvesting rate was higher than 90%, the unripe fruit drop rate was lower than 10%, and the damage rate was lower than 10%. The machine received attention from local coffee planters and satisfied the requirements for small-scale coffee harvesting in Yunnan Province.

## 8. Conclusions

This study investigated the effectiveness of vibrational harvesting of small-grain coffee fruit through the mechanical analysis, theoretical calculations, modeling and simulation, and field trials of coffee fruit abscission. The main conclusions of this study are as follows:

Images of vibrational shedding of the coffee fruit were obtained through high-speed photography that revealed the movement pattern of coffee fruit and branches during the vibration process. The pattern indicated that the coffee fruit-stalk joint is primarily subjected to tangential and normal tensile forces under the influence of forced vibrations. Furthermore, the analysis of vibrational shedding revealed that coffee fruit shedding is influenced by the vibration frequency, vibration amplitude, and excitation position on the branches. Accordingly, a handheld vibration coffee-picking device was designed. In addition, a rigid-flexible branch-machine coupling model was established to determine the optimal frequency, amplitude, and excitation position for coffee fruit shedding through single-factor simulation tests. Finally, a three-factor five-level quadratic regression orthogonal rotation combination test was performed to assess small-grain coffee harvesting with frequency, amplitude, and harvest rod excitation position as the test factors and ripening rate, unripe rate, and fruit damage rate as the test indicators. Through parameter optimization and experimental validation, optimal harvesting performance was achieved at a frequency of 62 Hz, vibration amplitude of 9 mm, and excitation position of 0.4 L. The ripening rate, growth rate, and damage rate were 92.22%, 8.33%, and 5.23%, respectively.

**Author Contributions:** Y.Y. and Q.L. proposed the theme of this study; Y.Y. and Y.C. designed, and Y.C., S.Z. and D.S. completed the experiments; Q.L., Z.S. and Q.Z. gave modifications to the experiments; Y.C. and Y.Y. wrote and revised the paper. All authors have read and agreed to the published version of the manuscript.

**Funding:** This research was funded by the National Natural Science Foundation of China 31960366, the National Key Research and Development Program (2017YFD0700600- 2017YFD0700604), and Major sciences of Yunnan Province Technical Special Project (2016ZF001, 2017ZF001, 2018ZC001-3, 2018ZC001-4, 2018ZC001-5).

**Institutional Review Board Statement:** Not applicable.

**Data Availability Statement:** The raw data required to reproduce these findings cannot be shared because the data also form part of an ongoing study.

**Acknowledgments:** The authors thank all the reviewers who participated in the Review.

**Conflicts of Interest:** The authors declare no conflict of interest.

## References

- Zhang, M.D.; Wang, R.F.; Li, Y.; Hu, Q.X.; Li, M.; Zhang, M.S.; Duan, C.C. Ecological suitability zoning of *Coffea arabica* L. in Yunnan Province. *Chin. J. Eco-Agric.* **2020**, *28*, 168–178. (In Chinese)
- Huang, J.; Lv, Y. Yunnan *Coffea arabica* L. *Plants* **1998**, *17*. (In Chinese)
- Zhu, Y.M.; Dou, X.D.; Wang, R.F.; Xie, M.E.; Huang, W.; Li, M. Climate change impact on the region suitable for *Coffea arabica* growth in Yunnan province. *Acta Meteorol. Sin.* **2021**, *79*, 878–887. (In Chinese)
- Oliveros Tascón, C.E.; Benítez Mora, R.; Álvarez Mejía, F.; Aristizábal Tórres, I.D.; Ramírez Gómez, C.A.; Sanz Uribe, J.R. Cosecha del café con vibradores portátiles del tallo. *Rev. Fac. Nac. Agron. Medellín* **2005**, *58*, 2697–2708.
- Araújo e Silva Ferraz, G.; De Silva, F.M.; de Carvalho Alves, M.; de Lima Bueno, R.; da Costa, P.A.N. Geostatistical analysis of fruit yield and detachment force in coffee. *Precis. Agric.* **2012**, *13*, 76–89. [[CrossRef](#)]
- Santos, F.L.; de Queiroz, D.M.; Pinto, F.; de Resende, R.C. Frequency and amplitude of vibration on coffee harvesting. *Rev. Bras. Eng. Agríc. Ambient.* **2010**, *14*, 425–431.
- De Gonzaga Ferreira Junior, L.; de Siva, F.M.; Ferreira, D.D. Displacement tracking of harvester rods of a coffee harvester. *IEEE Lat. Am. Trans.* **2017**, *14*, 4674–4680. [[CrossRef](#)]
- De Gonzaga Ferrera Júnior, L.; de Silva, F.M.; Ferreira, D.D.; Sales, R.S. Recommendation for mechanical harvesting of coffee based on vibration behavior settings rods harvesters. *Ciência Rural St. Maria* **2016**, *46*, 273–278.
- Snoeck, J.; Bernard Coffre, P.; Pechereau, M. La récolte mécanique du café à l'aide d'un fouetteur. *Café-Cacao-Thé* **1976**, *20*, 297–300. (In French)
- Tascón, F.G.; Uribe, C. Design of a shaker-clamp system for inertial shakers of coffee trees. In Proceedings of the ASAE Annual Meeting, St. Joseph, MI, USA, 1 October 2003.
- Cárdenas, E.L.M.; Tascón, C.E.O.; Mejía, F.Á. A portable device to assist in the harvest of coffee in colombia. *Rev. Fac. Nac. Agron. Medellín* **2015**, *68*, 7471–7479. [[CrossRef](#)]
- Coelho, A.L.F.; Santos, F.L.; Queiroz, D.M.; Pinto, F.A.C. Dynamic behavior of the coffee fruit-stem-branch system using stochastic finite element method. *Coffee Sci.* **2016**, *11*, 1–10.
- Yu, Y.J.; Wang, J.; Lai, Q.H.; Jia, G.X.; Yu, F.; Cao, Y. Design and experiment of hand-held vibrating comb-type *Coffea arabica* L. harvester. *Trans. Chin. Soc. Agric. Mach.* **2021**, *52*, 124–133. (In Chinese)
- Zong, W.Y.; Huang, M.C.; Xiao, Y.Y.; Li, M.; Deng, D.L. Design and experiment of the fruit-beating dropping device for chestnut harvesters. *Trans. CSAE* **2021**, *37*, 1–10. (In Chinese)
- Wu, D.L.; Li, C.; Cao, C.M.; Fan, E.B.; Wang, Q. Analysis and experiment of the operation process of branch-shaking type camellia oleifera fruit picking device. *Trans. CSAE* **2020**, *36*, 56–62. (In Chinese)
- Ji, W.; Qian, Z.; Xu, B.; Chen, G.; Zhao, D. Apple viscoelastic complex model for bruise damage analysis in constant velocity grasping by gripper. *Comput. Electron. Agric.* **2019**, *162*, 907–920. [[CrossRef](#)]
- Castro-García, S.; Blanco-Roldán, G.L.; Gil-Ribes, J.A.; Agüera-Vega, J. Dynamic analysis of olive trees in intensive orchards under forced vibration. *Trees* **2008**, *22*, 795–802. [[CrossRef](#)]
- Yu, P.; Li, C.; Takeda, F.; Krewer, G.; Rains, G.; Hamrita, T. Quantitative evaluation of a rotary blueberry mechanical harvester using a miniature instrumented sphere. *Comput. Electron. Agric.* **2012**, *88*, 25–31. [[CrossRef](#)]
- Blanco-Roldán, G.L.; Gil-Ribes, J.A.; Kouraba, K.; Castro-García, S. Effects of trunk shaker duration and repetitions on removal efficiency for the harvesting of oil olives. *Appl. Eng. Agric.* **2009**, *25*, 329–334. [[CrossRef](#)]
- Whitney, J.D.; Patterson, J.M. Development of a citrus removal device using oscillating forced air. *Trans. ASAE* **1972**, *15*, 849–855.
- Sessiz, A.; Özcan, M.T. Olive removal with pneumatic branch shaker and abscission chemical. *J. Food Eng.* **2006**, *76*, 148–153. [[CrossRef](#)]

22. Tang, Z.H.; Meng, X.; Shen, C.; Jia, S.; Zhou, Y.; Zheng, X.; Qin, Z. Design and experiment investigation of mechanical vibration tree fruits and nuts harvester. *J. Agric. Mech. Res.* **2010**, *32*, 65–69. (In Chinese)
23. Yang, H.Y.; Kan, Z.; Wang, L.H. Designing equipment of dwarf and close planting jujube harvest. *J. Agric. Mech. Res.* **2012**, *34*, 77–80. (In Chinese)
24. Lu, Z.P.; Xu, W. Research status and development trend of vibrating fruit and vegetable picking machinery. *For. Mach. Woodwork. Equip.* **2022**, *50*, 30–36. (In Chinese)
25. Zhang, Z.; Xiao, H.G.; Ding, W.Q.; Mei, S. Mechanism simulation analysis and prototype experiment of Lycium barbarum harvest by vibration mode. *Trans. Chin. Soc. Agric. Eng.* **2015**, *31*, 20–28. (In Chinese)
26. Wang, H.B.; Guo, Y.L.; Bao, Y.D.; Geng, L. Mechanism analysis and simulation of blueberry harvest by vibration mode. *Trans. Chin. Soc. Agric. Eng.* **2013**, *29*, 40–46. (In Chinese)
27. San, Y.L.; Yang, H.M.; Wang, X.N.; Guo, W.S.; Hou, S.L. Dynamic response analysis of apricot fruit dropping during vibration harvesting. *Trans. Chin. Soc. Agric. Eng.* **2018**, *34*, 68–75. (In Chinese)
28. Nakayama, H.; Sayama, H.; Sawaragi, Y. A generalized Lagrangian function and multiplier method. *J. Optim. Theory Appl.* **1975**, *17*, 211–227. [[CrossRef](#)]
29. Agrawal, O.P. Formulation of Euler–Lagrange equations for fractional variational problems. *J. Math. Anal. Appl.* **2002**, *272*, 368–379. [[CrossRef](#)]
30. Gao, Z.C.; Zhao, K.J.; Li, L.J.; Pang, G.Y.; Wang, X.C. Design and experiment of suspended vibratory actuator for picking Camellia Olerfera fruits. *Trans. Chin. Soc. Agric. Eng.* **2019**, *35*, 9–17. (In Chinese)
31. Silva Souza, V.H.; Dias, G.L.; Rezende, A.A.; Luis Gonçalves, S.A.; Lúcio Santos, C.F.; Magalhães, R.R. Evaluation of the interaction between a harvester rod and a coffee branch based on finite element analysis. *Comput. Electron. Agric.* **2018**, *150*, 476–483. [[CrossRef](#)]
32. Alistair John, S. Development of an Autonomous Kiwifruit Harvester. Ph.D. Thesis, Massey University, Manawatu, New Zealand, 2012.

**Disclaimer/Publisher’s Note:** The statements, opinions and data contained in all publications are solely those of the individual author(s) and contributor(s) and not of MDPI and/or the editor(s). MDPI and/or the editor(s) disclaim responsibility for any injury to people or property resulting from any ideas, methods, instructions or products referred to in the content.